Energy Proceedings
Vol 34, 2023
ISSN 2004-2965

Laboratory Study of Supercritical CO_2 Shock Fracturing in Hot Dry Rock: The Utilization of CO_2 in Geothermal Stimulation

Xiaoguang Wu, Wenchao Zou, Zhongwei Huang*, Haizhu Wang*, Gensheng Li, Xianzhi Song, Zixiao Xie

State Key Laboratory of Petroleum Resources and Prospecting, China University of Petroleum, Beijing 102249, China

(E-mail address: huangzw@cup.edu.cn; whz0001@126.com)

ABSTRACT

Carbon dioxide (CO_2) has great utilization potential in the exploitation of deep geothermal resources, especially hot dry rock (HDR). As a clean and renewable resource, HDR geothermal presents a promising prospect in meeting the growing demand for energy and achieving low-carbon solutions. To address the challenges posed in HDR development, such as large water consumption, simple fracture pattern and corresponding fast thermal breakthrough of Enhanced Geothermal System (EGS), a novel non-aqueous stimulation method which combines the advantages of supercritical CO_2 (SC) fracturing and dynamic shock effect is proposed and investigated in this paper, i.e. supercritical carbon dioxide shock (SCS) fracturing. To determine its stimulation performance in HDR, we performed controllable lab-scale SCS fracturing experiments on high-temperature granites subjected to true tri-axial stresses. By comparing with conventional water fracturing and SC-CO_2 fracturing, the fracture initiation behavior and stimulation performance of SCS fracturing were investigated quantitatively based on CT scanning and reinjection tests, with respect to fracture morphology and conductivity. Effects of critical parameters were analyzed as well, such as shock pressure, in-situ stress and rock temperature. Results indicate that the breakdown pressure of granite is 24.2~57.5% lower than the shock pressure during SCS fracturing, and it decreases with increasing rock temperature. SCS fracturing could create complex fracture network with more interconnected branches and larger seepage spaces. The volume, area and width of fractures by SCS fracturing are 545.3%, 98.4% and 126.3% higher than those of water fracturing, respectively. The fracture conductivity is 3.4~7.0 times and 4.5~21.2 times higher, as compared to water fracturing and SC fracturing. As the rock temperature increases, both the tortuosity and conductivity of fractures improve dramatically, which benefits to extend the flow path of working medium and enhance the heat transfer performance. In-situ stress plays a relatively weak role in controlling fracture propagation of SCS fracturing. At horizontal stress difference coefficient of 0.14~0.60, the fracture propagation behaves more randomly in direction, contributing to forming complex fractures with multi-branches. Higher shock pressure conduces to the stimulation performance enhancement of SCS fracturing, improving the complexity and connectivity of fracture networks, and promote the fracture to get rid of the control of in-situ stress in EGS. The key findings are expected to provide a novel insight into developing HDR geothermal in a more environmentally and more efficient way, and achieving CO_2 utilization and storage.

Keywords: Hot dry rock; CO_2 Utilization; EGS; Supercritical CO_2; Shock Fracturing

NONMENCLATURE

Abbreviations	
HDR	Hot dry rock
EGS	Enhanced geothermal system
CO_2	Carbon dioxide
SC-CO_2	Supercritical carbon dioxide
SCS	Supercritical carbon dioxide shock
CT	Computed tomography
SEM	Scanning electron microscope
XRD	X-ray diffraction
EDS	Energy dispersive system
SNR	Signal–noise ratio
TNT	Trinitrotoluene

This is a paper for International CCUS Conference 2023 (ICCUSC2023), April 14-15, 2023, Beijing, China.

Symbols	
T_r	Temperature of rock
Q	Flow rate
P_s	Shock pressure
σ_h	Minimum horizontal stress
σ_H	Maximum horizontal stress
σ_v	Vertical stress
C_f	Fracture conductivity
q_w	Injection rate
μ	Viscosity of reinjection fluid
r_e	Effective radius
r_w	Wellbore radius
ΔP_{wf}	Pressure difference between the wellbore and fracture
E	Blasting energy
W_{TNT}	Explosion equivalent
P	Shock pressure
V	Volume of blasting tube
k	Adiabatic coefficient
Q_{TNT}	Explosion energy of 1kg trinitrotoluene

1. INTRODUCTION

Geothermal energy is a renewable and sustainable resource which plays an important role in meeting the growing demand for energy and achieving low-carbon solutions [1]. Hot dry rock (HDR), as a typical type of geothermal resources, offers great potential of thermal energy. The HDR reservoir is characterized by the rocks with naturally low permeability and high temperature ranging from 150~650 ℃, located at 3~10 km depth below the earth's surface [2, 3]. To enhance the permeability of HDR and extract geothermal quantities capable of producing electricity economically, hydraulic fracturing is generally employed to stimulate the reservoir and create pathways for working fluid flow and heat extraction between injection wells and production wells, also referred as enhanced geothermal system (EGS). In EGS, creating an inter-connected and highly conductive fracture network is the foundation for obtaining enough heat transfer spaces and high flow rates of working fluid in the reservoir [3, 4]. However, there are several challenges for conventional hydraulic fracturing in EGS, such as high breakdown pressure and simple fracture morphology [5, 6]. The lessons learned from previous EGS projects like Fenton Hill in US, Hijiori in Japan, Rosemanowes in England and etc. indicate that the simple 2-D planar fracture pattern created by conventional hydraulic fracturing is not desirable for HDR in most cases [6-8], which could result in fast thermal breakthrough and shorten the service life of EGS significantly. Additionally, the conventional water-based fracturing fluid also poses challenges for the environment, due to the chemical additives and massive water consumption [9-11]. Hence, finding a non-contamination and non-aqueous based fracturing method which could create 3-D complex inter-connected fracture networks, is the key to realize the effective stimulation of HDR and economic development of EGS.

To address issues above, the supercritical carbon dioxide (SC-CO_2) shock fracturing was proposed in this paper to apply in the HDR geothermal stimulation. In this method, CO_2 is used as an alternative to water-based fracturing fluid and injected into a specially designed downhole energizing device, in which the static pressure accumulates under the joint action of continuous injection and volume expansion of compressible fluid at high temperatures. Once the accumulated pressure exceeds the threshold value, the drainage channels of the downhole devices are opened to release controllable high-pressure shock waves instantly and crack the surrounding rocks, creating a volumetric fracture zone near wellbore. As the CO_2 continues to be injected in the wellbore, these blasted fractures can be further expanded, forming a large-scale complex fracture network. Since the CO_2 has a relatively low critical temperature and pressure (304.13K and 7.38 MPa), it keeps at supercritical state during the stimulation process of HDR.

The SC-CO_2 shock (SCS) fracturing, as a non-aqueous stimulation method, could offer potential solutions to the challenges mentioned above. This technique combines the advantages of SC-CO_2 fracturing and dynamic shock effect. Firstly, SC-CO2 has the features of low viscosity and high permeability, which makes it easier to penetrate tight rocks and induce multi-branch fractures [12, 13]. Next, the hot dry rock is mainly brittle granite which has low resistance to the instantaneous dynamic loading. When the dynamic shock wave is coupled, the complexity and connectivity of the fracture networks can be further enhanced, improving the stimulation performance significantly [14]. Moreover, the near-wellbore fracture zone induced by shock blasting can effectively reduce the skin factor and improve the injection capacity of EGS [15]. Injection capacity is a key engineering parameter indicating the effectiveness of EGS. A high injection capacity represents high flow flux and heat extraction capacity in the reservoir. EGS could be considered as economical development only when the injection capacity reaches 50 kg/s [16]. In addition,

taking CO_2 as the substitution of conventional water-based fracturing fluid can not only eliminate the environmental risks mentioned above, but achieve CO_2 utilization and storage, providing a potential decarbonization solution [17, 18].

In fact, the stimulation enhancement mechanism of SC-CO_2 shock fracturing is similar with CO_2 blasting fracturing technique, which has already been widely used in mining, especially in the coalbed methane recovery. Priors implemented comprehensive investigations on the borehole pressure evolution [19-22], explosion energy [22, 23], shock wave [24, 25] and fracture propagation [26-29] of CO_2 blasting fracturing experimentally and numerically. Field tests indicate that the quantity of gas extraction from a single borehole controlled by fracturing increased by about 4 times in the initial 8 hours after CO_2 blasting [30]. However, due to the relatively shallow burial depth of coal seam, CO_2 exists in liquid phase rather than supercritical state during the fracturing process. As compared to liquid CO_2, supercritical CO_2 has very different physical properties, and thereby shows a great difference in the fracturing performance [31]. Additionally, unlike coalbed methane formations, HDR is characterized by high-temperature in nature. Intense heat transfer and thermal stresses are involved in the dynamic blasting process. Previous literatures studied the fracturing propagation and heat extraction capacity of CO_2 fracturing in EGS [32-35], but most of them implemented CO_2 injection in the quasi-static mode, which is quite different from SCS fracturing. The combined effect of thermal stress and dynamic shock was rarely reported. The stimulation performance of SCS fracturing under the joint action of thermal stress and dynamic shock loading are still unclear.

To determine the stimulation performance and feasibility of SC-CO_2 shock fracturing in EGS, we conducted controllable lab-scale SC-CO_2 shock fracturing experiments on high-temperature granites subjected to true tri-axial stresses. Conventional water fracturing and SC-CO_2 fracturing were also conducted as comparisons. Borehole pressure evolution was record and analyzed. The stimulation performances of the three fracturing methods were evaluated and contrasted quantitatively based on X-ray Computed Tomography (CT) scanning and reinjection tests, with respect to stimulated volume, fracture morphology and conductivity. Scanning electron microscope (SEM) was used to observe micro-failure structures. Effects of several critical parameters on the fracturing performance were investigated as well, such as shock pressure, tri-axial stress and rock temperature. The key findings are expected to provide a methodological and theoretical guidance for developing HDR geothermal in a more environmentally and more efficient way, and achieving CO_2 utilization and storage.

2. MATERIAL AND METHODS

2.1 Sample preparation

The rock material used in our experiments is granite collected from the Qiabuqia basin of Qinghai Province, which is a potential HDR project site in China. According to the X-ray diffraction (XRD) analysis as shown in Table 1, the granite is mainly composed of quartz (28.6%), orthoclase (17.3%), plagioclase (42.9%) etc., in which the brittle materials occupy the majority. Basic mechanical properties of the granites were tested as well, as shown in Table 2. Before experiments, we cut the granites into cubes with the dimension of 100 mm in side length, as illustrated in Fig. 1. A centered hole with 16 mm in diameter and 60 mm in depth was drilled in the sample to simulate the wellbore. A stainless-steel casing extending 40 mm into the wellbore was cemented using the temperature resistant epoxy-resin adhesive, with a 20 mm open-hole section left. A piezometric sensor was set in the borehole to capture and record the pressure signals during the fracturing experiment, with the data acquisition rate of 1000 s^{-1}.

Table 1 XRD test results of the mineral composition of granite.

Minerals	Quartz	Orthoclase	Plagioclase	Dolomite	Pyroxene	Clay minerals
Proportion	28.6%	17.3%	42.9%	2.3%	5.5%	3.4%

Table 2 Physical and mechanical properties of granite.

Properties	Density (kg/m3)	Permeability (mD)	UCS (MPa)	Young's Modulus (GPa)	Poison's ratio	Tensile strength (MPa)
Values	2753±15	0.0069±0.001	153±10	34.2±2.1	0.19±0.08	10.3±0.08

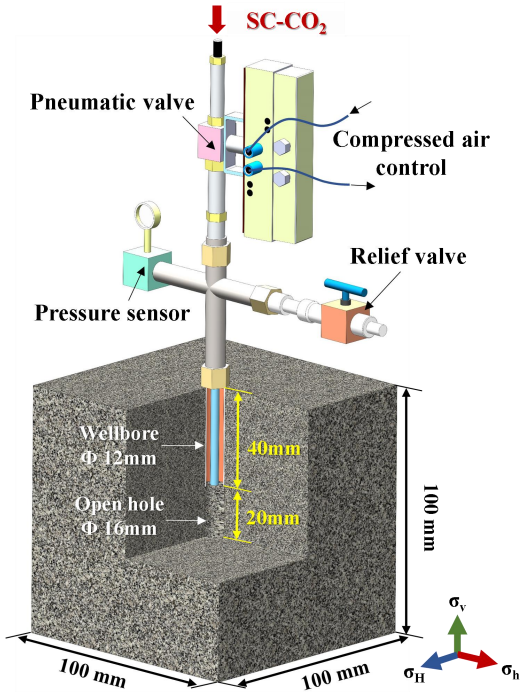

Fig. 1 Granite sample and wellbore setup.

2.2 Experimental setup and procedure

The lab-scale SC-CO_2 shock fracturing in HDR is a complex process involving in generating a supercritical environment for the fracturing fluid and simulating the in-situ temperature and stress conditions of rocks simultaneously. In this work, a true triaxial SC-CO_2 shock fracturing equipment of high-temperature rocks was designed and developed independently, as shown in Fig. 2 and Fig. 3, in which different stimulation experiments, such as SC-CO_2 fracturing, SC-CO_2 shock fracturing and water fracturing, can be carried out for rocks with different temperatures and stress. This equipment consists of five main modules, such as SC-CO_2 generation, shock pressure control, true-triaxial stress loading, rock heating and temperature control, and data acquisition. The SC-CO_2 generation, shock pressure control, triaxial loading module of high-temperature rocks are three unique modules differing from conventional triaxial fracturing experiment system.

High-pressure SC-CO_2 generation module (as shown in Fig. 2a). This module is designed to produce high-pressure SC-CO_2 to pressurize the borehole. CO_2 reaches the supercritical state when the pressure and temperature exceeds 7.38 MPa and 304.13 K, respectively. To simulate the supercritical environment, CO_2 gas is pneumatically compressed by supercharger and then stored in an energy accumulation tank with a volume of 3000 mL. Fluid in this tank is heated by circulating water-bath, and temperature sensors are used to realize the feedback regulation and real-time control of the temperature. Maximum heating temperature of the fracturing fluid is 100℃.

Shock pressure control module. Unlike conventional hydraulic fracturing with stable and slow injection in the borehole, high-pressure SC-CO_2 is released by the pneumatic valve into the borehole within milliseconds to induce shock waves and fractures. In this module, a screw air compressor is combined with the supercharger to energize the CO_2 fluid with a pressurization ratio of 1:140, as shown in Fig. 2b. Max shock pressure of our device can reach 100 MPa.

True triaxial loading module of high-temperature rocks (as shown in Fig. 2c and 2d). This module is designed for the sample with the dimensions of 100~400 mm cubes. Triaxial stress up to 50 MPa can be loaded on the sample along x-axis, y-axis, and z-axis with an accuracy of ±0.1 MPa. To simulate the high-temperature conditions of HDR, 36 electric heating devices with a total power of 14.4 kW are uniformly arranged in the surrounding plate of triaxial loading unit, and temperature sensors are used to realize the monitoring of thermal loading and temperature feedback regulation of rock samples. The maximum heating rate can reach 100 ℃ /h, but the maximum heating temperature generally does not exceed 200 ℃ for the safety of equipment. For the purpose of

improving experimental efficiency, we preheated the rock samples to the target temperature in muffle furnace with a slow heating rate of 5 ℃ /min in this work, and then transfer to the triaxial stress loading unit for the temperature control.

Fig. 2 Ture triaxial fracturing equipment for SC-CO_2 shock in high-temperature rocks. (a) High-pressure SC-CO_2 generation module; (b) Shock pressure control module; (c) Ture triaxial-loading module; (d) Rock temperature control in the confining kettle.

The procedure of SC-CO_2 shock fracturing includes rock heating, triaxial stress loading, fluid pressurization, water-bath circulation heating and energy release for blasting, which are detailed as follows:

① Place the core that was slowly heated to the target temperature in advance in Muffle furnace quickly into the triaxial loading unit. A slow heating rate of 5℃ /min was set for the furnace to prevent from thermal shock during heating;

② Heat the rock and control the temperature by using the electric heat tubes and thermocouples;

③Turn on the true triaxial loading device, and load the triaxial stress according to the predetermined scheme;

④ Start the air compressor to drive the supercharger (gray dotted block in Fig. 3), and charge the CO_2 from the cartridge into the high-pressure container and pressurize it (flow along the blue arrow in Fig. 3);

⑤ Turn on the water-bath heater to heat and control the temperature of high-pressure CO_2 in the container by circulating water (flow along the black arrow in Fig. 3), and keep CO_2 in the supercritical state, with the temperature of 60 ℃ and pressure ranging from 14 to 24MPa;

⑥ When the pressure of CO_2 in the container reaches the predetermined value, the pneumatic valve can be remotely opened through the air compressor to realize the instantaneous release of high-pressure supercritical CO_2 into the borehole (flow along the red arrow) and complete the stimulation of high-temperature rock sample. The data during the whole fracturing process such as temperature, pressure and triaxial stress can all be monitored by the data acquisition system;

⑦Turn off the supercharge, water circulation pump and rock heating devices after experiments. Release the triaxial stresses and take out the rock sample for further analysis.

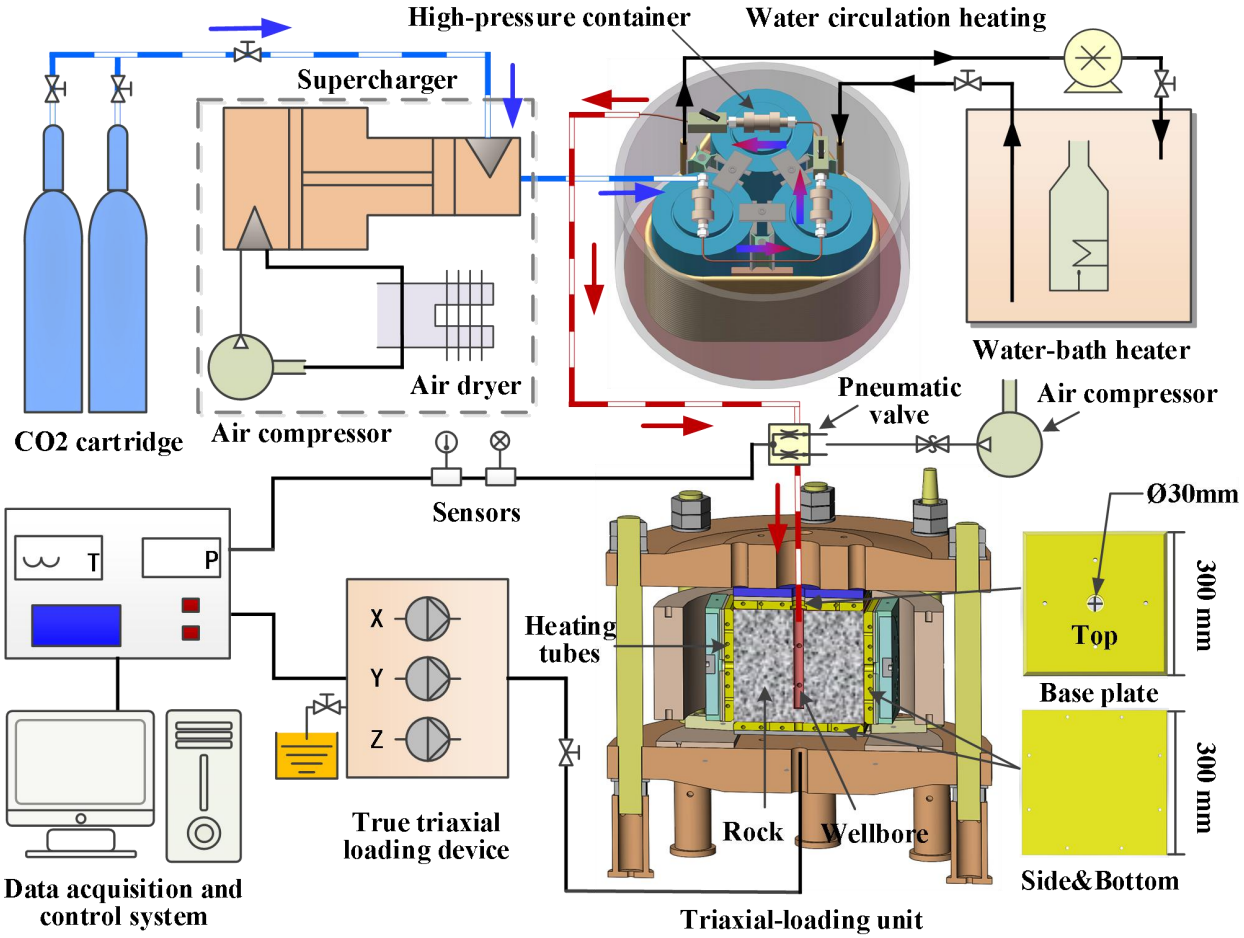

Fig. 3 Schematic of the true triaxial SC-CO_2 shock fracturing system.

After the fracturing experiments, X-ray computed tomography (CT) scanning was conducted on the granite samples to obtain the post-treated 2D slices, which could be stacked mathematically to reconstruct the 3D skeleton of fracture networks. In this study, the high-resolution computed tomography (CT) inspection system YXLON FF85 was used. The applied YXLON Panel detector has a detection range of 1848mm×1848mm, with a frame rate up to 100 fps. The distance from the ray focus to the detector and to the object being scanned was set to 4600mm and 3780mm, respectively. In addition, to reveal the microscopic cracking mechanism of granite, a FEI Quanta 200F scanning electron microscope (SEM) and Energy Dispersive System (EDS) was used to observe microstructural failures. The maximum magnification of this machine is up to ×200000.

2.3 Experiment scheme

Table 3 shows the experiment scheme of this study. Totally 20 granite samples in 6 groups were tested under different triaxial stress and temperature conditions, with different fracturing methods. Samples in SCS 1-1~1-5, SCS 2-1~2-3, SCS 3-1~3-4 were used to perform the SC-CO_2 shock fracturing tests on rocks with different temperatures (25~180 ℃) under the shock pressures of 14~24 MPa, while SCS 3-3, 4-1 and 4-2 were used to determine the effect of triaxial stress on the SC-CO_2 shock fracturing. Three different tri-axial stress conditions were investigated, with the horizontal stress difference ratio ranging from 0.14 to 1.67. To better evaluate the performance of the SC-CO_2 shock fracturing and identify its characteristics in fracture initiation and propagation, samples W-1~W-3 and SC-1~SC-3 were taken as comparisons in this study, to conduct water fracturing and conventional SC-CO_2 fracturing on rocks with different temperatures. A constant injection rate of 10ml/min was applied in the water fracturing. After the tests, the samples SCS 1-3, SC-1 and W-1 were scanned by CT to reconstruct their 3-D fracture networks for quantitative analysis and comparison between different fracturing methods.

Table 3 Experimental matrix for water fracturing, SC-CO_2 fracturing and SC-CO_2 shock fracturing on high-temperature granite.

Sample No.	Fracturing type	Shock pressure Or Injection rates	$\sigma_H/\sigma_h/\sigma_v$ (MPa)	Horizontal stress difference ratio $(\sigma_H-\sigma_h)/\sigma_h$	Granite temperature (℃)
SCS 1-1	SC-CO_2 shock fracturing	14 MPa	8/5/10	0.6	25
SCS 1-2	SC-CO_2 shock fracturing	16 MPa	8/5/10	0.6	25
SCS 1-3	SC-CO_2 shock fracturing	18 MPa	8/5/10	0.6	25
SCS 1-4	SC-CO_2 shock fracturing	20 MPa	8/5/10	0.6	25
SCS 1-5	SC-CO_2 shock fracturing	24 MPa	8/5/10	0.6	25
SCS 2-1	SC-CO_2 shock fracturing	16 MPa	8/5/10	0.6	100
SCS 2-2	SC-CO_2 shock fracturing	20 MPa	8/5/10	0.6	100
SCS 2-3	SC-CO_2 shock fracturing	24 MPa	8/5/10	0.6	100
SCS 3-1	SC-CO_2 shock fracturing	16 MPa	8/5/10	0.6	180
SCS 3-2	SC-CO_2 shock fracturing	18 MPa	8/5/10	0.6	180
SCS 3-3	SC-CO_2 shock fracturing	20 MPa	8/5/10	0.6	180
SCS 3-4	SC-CO_2 shock fracturing	24 MPa	8/5/10	0.6	180
SCS 4-1	SC-CO_2 shock fracturing	20 MPa	8/3/10	1.67	180
SCS 4-2	SC-CO_2 shock fracturing	20 MPa	8/7/10	0.14	180
W-1	Water fracturing	10 ml/min	8/5/10	0.6	25
W-2	Water fracturing	10 ml/min	8/5/10	0.6	100
W-3	Water fracturing	10 ml/min	8/5/10	0.6	180
SC-1	SC-CO_2 fracturing	/	8/5/10	0.6	25
SC-2	SC-CO_2 fracturing	/	8/5/10	0.6	100
SC-3	SC-CO_2 fracturing	/	8/5/10	0.6	180

3. RESULTS AND ANALYSES

3.1 Pressure evolution in the wellbore

To determine the fracture initiation behaviors, we record the pressure in the borehole in real time during the fracturing process of different methods. The borehole pressure evolution curves of water fracturing, SC fracturing and SCS fracturing are plotted versus time in Fig. 4a, 4b and 4c, respectively. It is found that the borehole pressure of water fracturing increases gradually, followed by a sudden drop, indicating the initiation of fracture at the peak pressure (breakdown pressure), and then stabilized in a certain pressure value. Unlike water fracturing, SC fracturing presents a moderate pressure drop rate after the peak, which may be attributed to the relatively narrow fracture as compared to water fracturing. Note that high-pressure SC-CO_2 was pushed by CO_2, so that the pressurization of SC-CO_2 started at a relatively high pressure.

The pressure evolution of SCS fracturing differs from that of water fracturing and SC fracturing greatly. In the SCS fracturing, the borehole pressure reaches to the peak rapidly in a few hundred milliseconds, applying a dynamic load in the wellbore, and then drops to 0MPa in a stepwise manner in several seconds. The whole fracturing period is less than 10 seconds, which is significantly shorter than those of water fracturing and SC fracturing. There are multiple short pressure plateaus in the curves due to the joint action of the pressure wave reflection and hedging in the borehole and the fracture propagation, consistent with previous studies [20]. Moreover, it is noted that the granite breaks at a peak pressure value that is 24.2~57.5% lower than the shock pressure during SCS fracturing. The rock temperature has a great influence on the breakdown pressure, as illustrated in Fig. 4d. The breakdown pressure decreases with increasing rock temperature for the three fracturing methods. As compared to the granite at 25℃, the breakdown pressure of granite at

180 ℃ reduces by 50.3%, 14.2% and 44.3% for water fracturing, SC fracturing and SCS fracturing, respectively. This fact is mainly attributed to the higher thermal stress induced by greater temperature difference between fracturing fluid and rocks, which facilitate the initiation of fractures. Among the three fracturing methods, SC fracturing has the lowest breakdown pressure for granite samples with the same temperature, substantiating that the low-viscosity and low-density supercritical fluid benefits to lower the breakdown pressure of granite. Although the working medium for both SC fracturing and SCS fracturing is supercritical fluid, the heat transfer and corresponding thermal stress in the SCS fracturing are weaker than those in SC fracturing due to the short fracturing period, thereby leading to a relatively higher breakdown pressure in SCS fracturing.

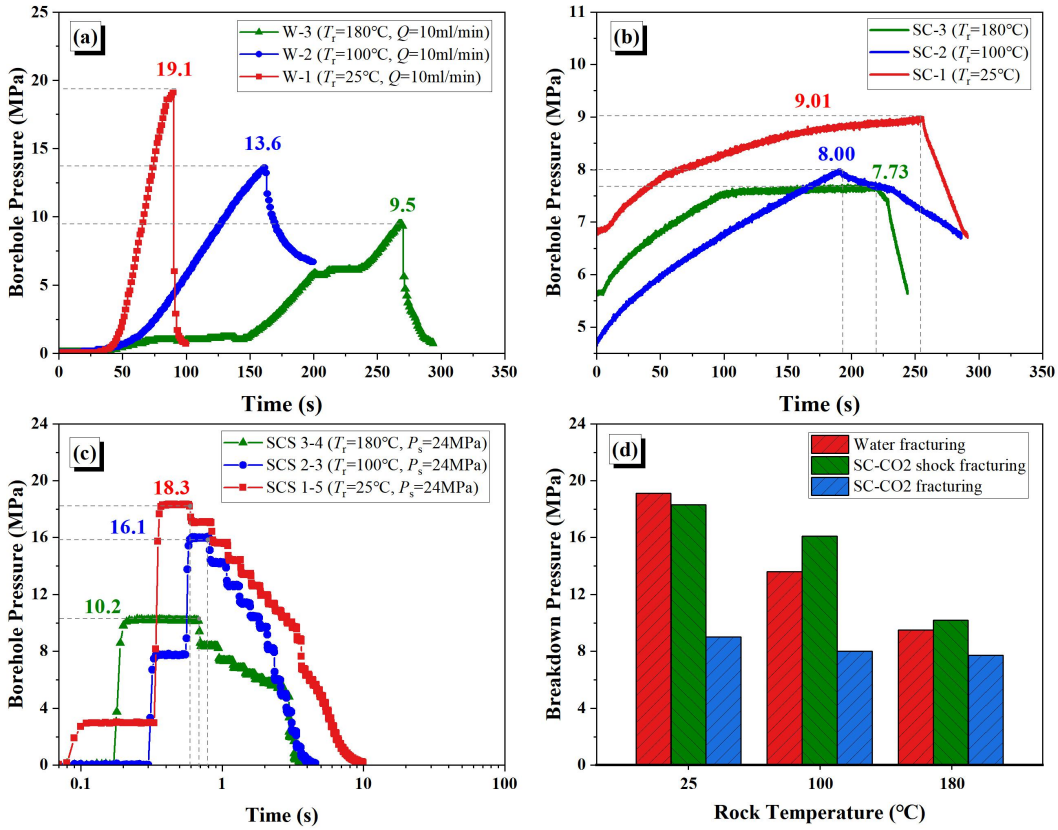

Fig. 4 Borehole pressure curves of different fracturing methods in granites with different temperatures, (a) Water fracturing; (b) SC-CO_2 fracturing; (c) SC-CO_2 shock fracturing with the shock pressure of 24 Mpa; (d) Comparison in the breakdown pressure between water fracturing, SC-CO_2 fracturing and SC-CO_2 shock fracturing. T_r represents the temperature of rock. Q represents the flow rate. P_s represents the shock pressure.

3.2 Fracture propagation pattern

Fracture propagation pattern directly determines the volume of artificial heat extraction space in EGS and the connectivity between injection well and production well, which is the key to measure the effectiveness of geothermal reservoir stimulation. However, narrow fractures on the granite are sometimes not noticeable and even invisible after tests. To better identify the fracture pattern and evaluate the conductivity of the fracture networks after fracturing, we reinjected dye solution into the granite samples with a flow rate of 20ml/min in the absence of confining stress, and marked the leaking areas in blue to highlight the fracture propagation path. Fig. 5 shows the fracture patterns in granite samples subjected to SCS fracturing under different rock temperature conditions. Although the SCS fracturing is an instantaneous loading process, the rock temperature could still have a positive effect on its stimulation performance. As compared to the granite samples of 25 ℃ as shown in Fig. 5a, high-temperature granites shown in Fig. 5b and 5c are more likely to form complex fracture networks under the same shock pressure, with more interconnected branches and larger seepage spaces created, indicating that the SCS fracturing may have a better applicability in

HDR reservoirs. Furthermore, the shock pressure is an important factor influencing the fracturing pattern as well. As expected, the complexity and connectivity of fracture networks improve significantly with increasing shock pressure, and the effect of shock pressure will be further detailed in the subsequent section 3.4.

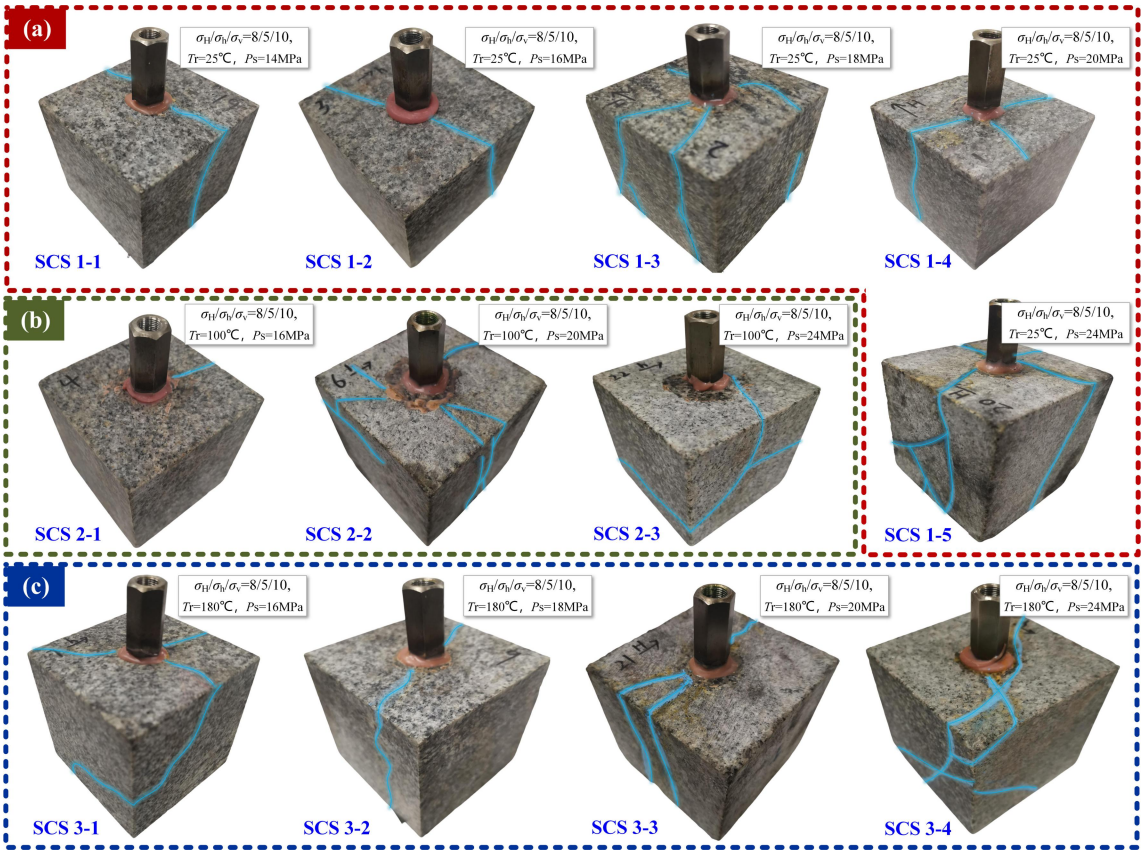

Fig. 5 SC-CO_2 shock fracturing performance in granites with different temperature and shock pressure, (a) Granite samples at 25℃; (b) Granite samples at 100℃; (c) Granite samples at 180℃.

To better illuminate the feature of the fracture propagation after SCS fracturing, the fold-out diagrams showing six surfaces of the treated granite cubes at the temperature of 25, 100 and 180℃ are plotted in Fig. 6a~6c, and contrasted with those after water fracturing and SC fracturing as shown in Fig. 6d~6f and Fig. 6g~6i, respectively. The stress coordinates in these figures represents the tri-axial stress loading directions from the top view of the granite samples. By comparing different fracturing methods, it can be found that the fracture created by SCS fracturing has more branches under the same rock temperature and stress conditions, forming a fracture network with significantly higher complexity and connectivity. Unlike water fracturing and SC fracturing, SCS fracturing shows merits in getting rid of the control of in-situ stress, and the fracture can propagate in a more random direction. In addition to the direction of maximum principal stress, several fracture branches even propagate along the minimum principal stress direction in SCS fracturing as shown in Fig. 6a~6c. Moreover, rock temperature has a great influence on the tortuosity of the fracture. As the temperature of rock increases, the tortuosity of fractures improves significantly. For granite samples at 25℃, the fracture of water fracturing and SC fracturing basically propagates along the direction of maximum principal stress, resulting in a relatively straight fracture plane. Nevertheless, for granite samples at 100℃ and 180℃, the fracture deflects from the maximum principal stress direction remarkably. A more curved fracture was created under high temperature conditions, which increases the tortuosity dramatically. The complex interconnected fracture network with high tortuosity in SCS fracturing benefits to extend the flow path of working medium, enhance the heat transfer performances, and prolong the serving life of EGS in the HDR geothermal reservoir.

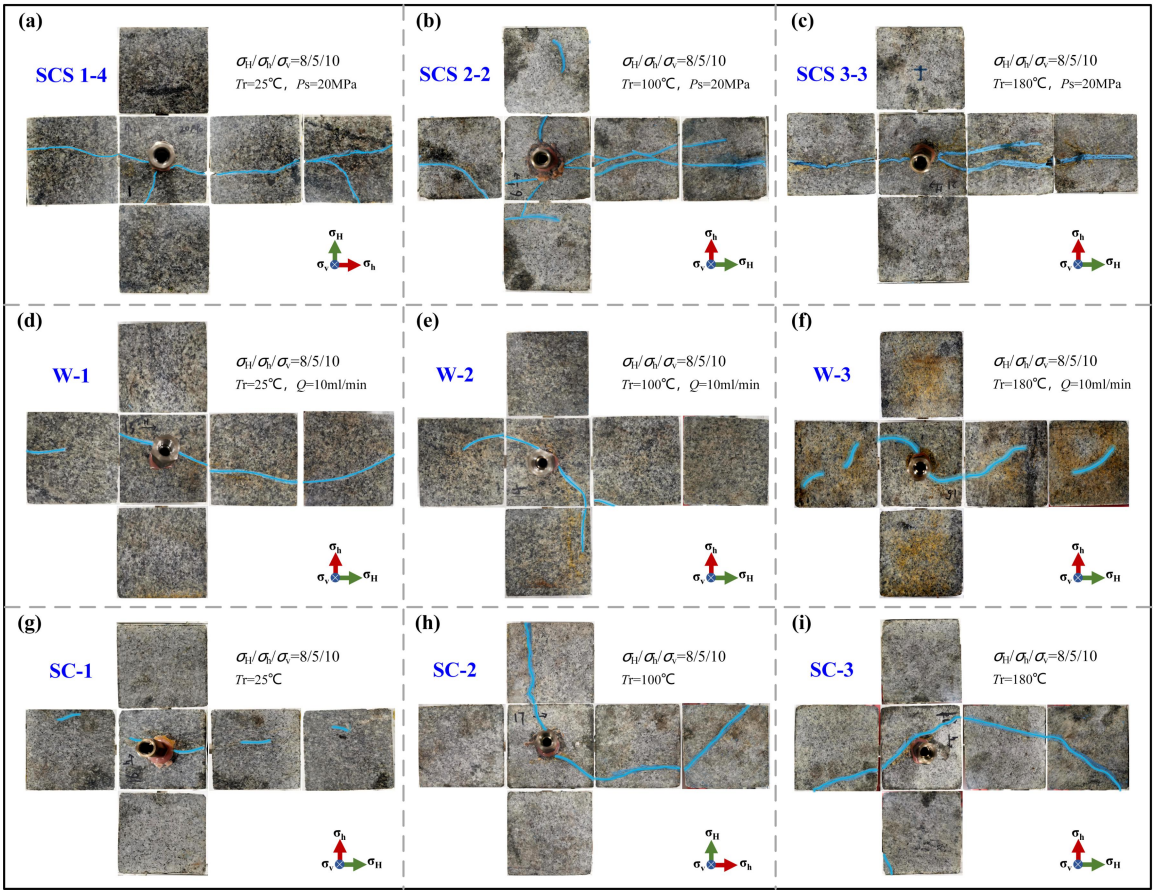

Fig. 6 Comparison in fracture patterns between various fracturing methods under different rock temperatures, (a) SC-CO_2 shock fracturing of granite at 25℃; (b) SC-CO_2 shock fracturing of granite at 100℃; (c) SC-CO_2 shock fracturing of granite at 180℃; (d) Water fracturing of granite at 25℃; (e) Water fracturing of granite at 100℃; (f) Water fracturing of granite at 180℃; (g) SC-CO_2 fracturing of granite at 25℃; (h) SC-CO_2 fracturing of granite at 100℃; (i) SC-CO_2 fracturing of granite at 180℃.

3.3 Fracture morphology characterization

Fracture morphology is a critical indicator for the stimulation performance and heat extraction capacity in EGS. To characterize the 3D morphology of fractures in granites quantitively, we conducted CT scanning on the fractured samples and obtain the post-treated 2D grayscale slices. Due to the relatively small fracture width of granites subjected to SC fracturing, fractures in the samples can not be identified by CT scanning system. Hence, only the scanning images of granite samples subjected to water fracturing and SCS fracturing were presented and contrasted, as shown in Fig. 7a and 7b. Unlike the matrix, the fractures present higher grayscale value, which can be observed clearly in these 2D slices. Water fracturing creates a simple two-wing fracture, consistent with the fracture propagation pattern described above. In contrast, the number, width and complexity of fractures formed by SCS fracturing are significantly higher than that of water fracturing. Two characteristic zones are created by SCS fracturing, i.e. near-wellbore crush zone and fracture radial extension zone. In the former zone, the granite is cracked remarkably, and multiple fractures crossed each other to form a fracture network, greatly reducing the skin coefficient near the wellbore. This zone contributes to a significant growth in EGS injection capacity and corresponding heat recovery. In the later zone, multiple outward-radiating fractures are created, which will be further extended by the subsequent continuous injection to connect the injection well and production wells. The shock waves weaken the control degree of in-situ stress and increase the randomness of fracture propagation direction. Compared with the single simple fracture created by water fracturing, the multiple randomly radiating extended fractures created by SCS fracturing can greatly enlarge the heat extraction space. Moreover, these randomly radiating extended fractures could communicate with more natural fractures and enhance the heat recovery performance more significantly.

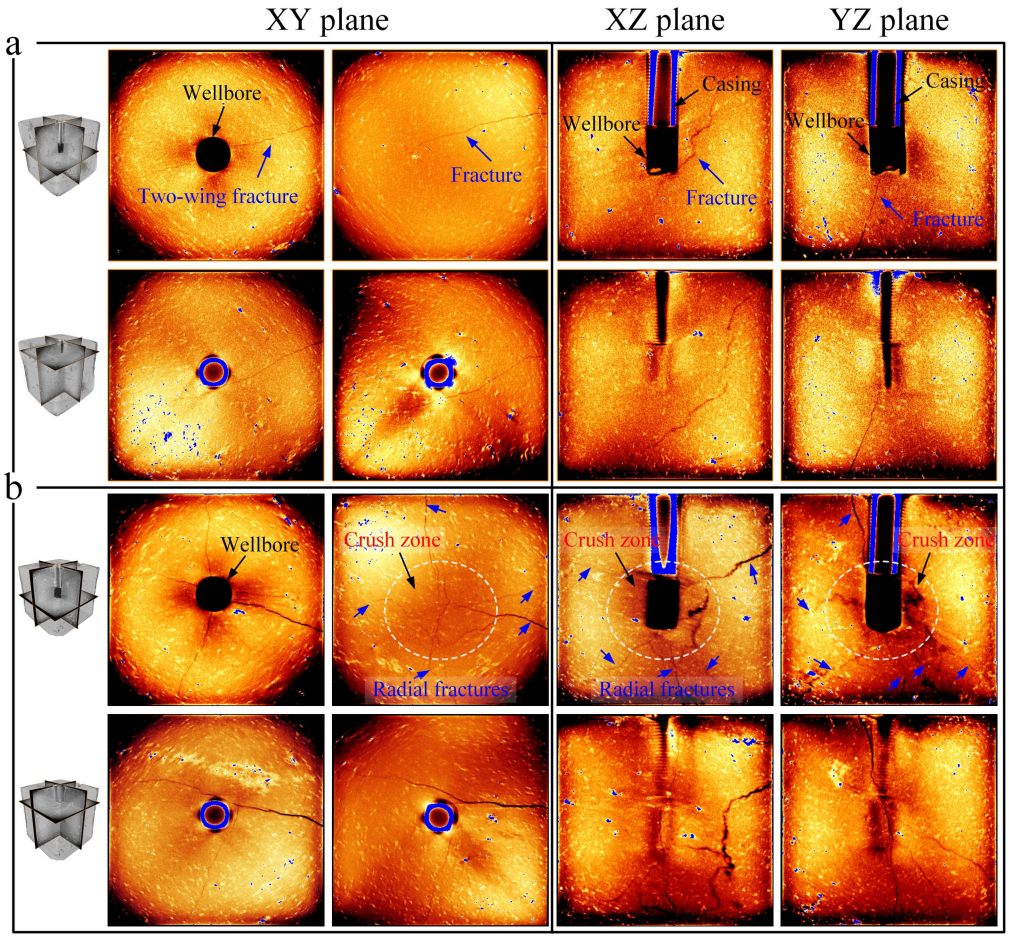

Fig. 7 X-ray 2D CT slices of granites treated by (a) water fracturing and (b) SC-CO_2 shock fracturing.

Based on the digital core analysis approach, the post-treated 2D slices were stacked mathematically to reconstruct the 3D matrix-fracture structures. To get rid of image noise and increase the signal–noise ratio (SNR), the images were denoised by using a non-local means filter. The 3D reconstructed fractures of granites treated by water fracturing and SCS fracturing are shown in Fig. 8a and 8b, respectively, and critical geometric parameters of fractures, such as fracture volume, surface area, average fracture width, fractal dimension and flatness, are calculated and given in Fig. 9. The fractures formed by hydraulic fracturing are straight and simple, basically along the direction of maximum principal stress, as shown in Fig. 8a. The fracture morphology formed by SCS is more complex, as shown in Fig. 8b, with multiple main fractures intersecting with each other and presenting high tortuous features. The fractal dimension factor is commonly used to describe the regularity and roughness of fracture morphology, indicating how complex the surface is and how it fills the space. The less smooth the surface is, the bigger the fractal dimension. As shown in Fig. 9, the fractal dimension of SCS fracture is 4.7% higher than that of water fracture, which further indicates that the fracture complexity is higher. Furthermore, SCS fracturing results in significantly larger heat extraction space. The volume, area and width of fractures by SCS fracturing are 545.3%, 98.4% and 126.3% higher than those of water fracturing, respectively.

Roughness is an important geometrical parameter to evaluate fracture morphology. The fracture with higher roughness has better self-supporting performance during shear-slipping, forming flow channels with higher conductivity and heat recovery effect. Herein, based on the reconstructed fractures, the flatness of fractures after hydraulic fracturing and SCS fracturing was extracted to characterize the roughness of fractures in the Thermo Scientific Avizo software, as shown in Fig. 9. Since the fracture by SCS fracturing has a more remarkable fluctuation surface and an obviously higher tortuosity (see Fig. 8), the flatness of fracture by SCS fracturing is an order of magnitude higher than that of water fracturing. Therefore, the fractures formed by SCS fracturing are more likely to form self-support in the shear slip

process, which improves the conductivity of the fractures and the heat recovery effect.

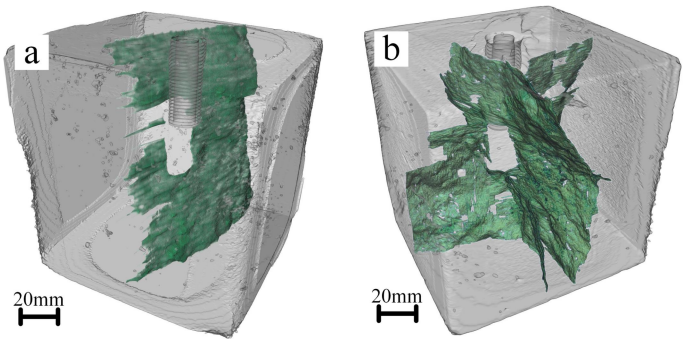

Fig. 8 Comparison in the 3D reconstructed fracture morphology of granites treated by (a) water fracturing and (b) SC-CO_2 shock fracturing.

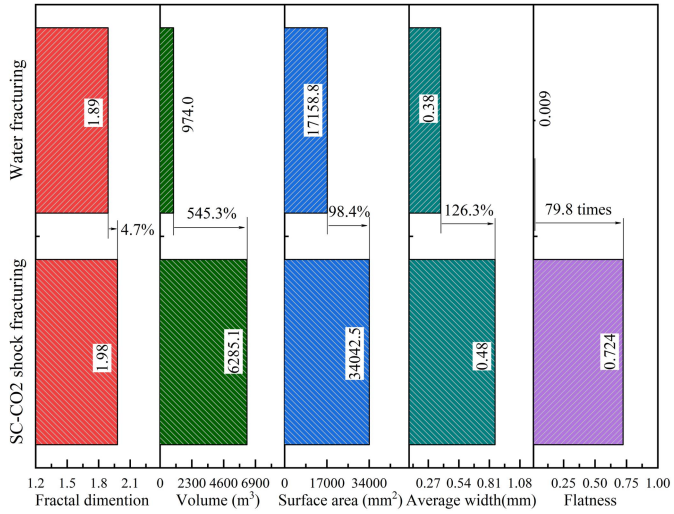

Fig. 9 Comparison in fracture geometry parameters between SC-CO_2 shock fracturing and water fracturing.

By using SEM with the maximum magnification of ×200000, micro failure structures of granites subjected to water fracturing, SC fracturing and SCS fracturing were observed, and EDS was also implemented to analyze the elements and minerals, as shown in Fig. 10. For water fracturing and SC fracturing, the pressure in the wellbore is loaded in a quasi-static mode, increasing at a relatively slow rate. Consequently, fracture propagates preferentially along the boundaries between minerals, which has lower strength as compared to the mineral particle itself. Inter-granular fractures play a more dominant role in the microscopic failure mode of water fracturing and SC fracturing. It is noted that the fracture aperture of SC fracturing is much smaller than that of the other two fracturing, at tens of microns level. It explains why fractures in granites subjected to SC fracturing are difficult to be effectively identified by CT scanning, as we mentioned above. In contrast, SCS fracturing is characterized by larger fracture aperture (on the order of a few hundred microns) and more trans-granular fractures. This fact is mainly attributed to the rich abundance of brittle minerals in granite, such as quartz, orthoclase and plagioclase as illustrated in Table 1, which has low resistance to the transient dynamic loading. During the SCS fracturing process, the wellbore pressure rises to the maximum within 1s, applying a dynamic shock load on the granite, thus inducing cracking of brittle minerals and generating more trans-granular fractures.

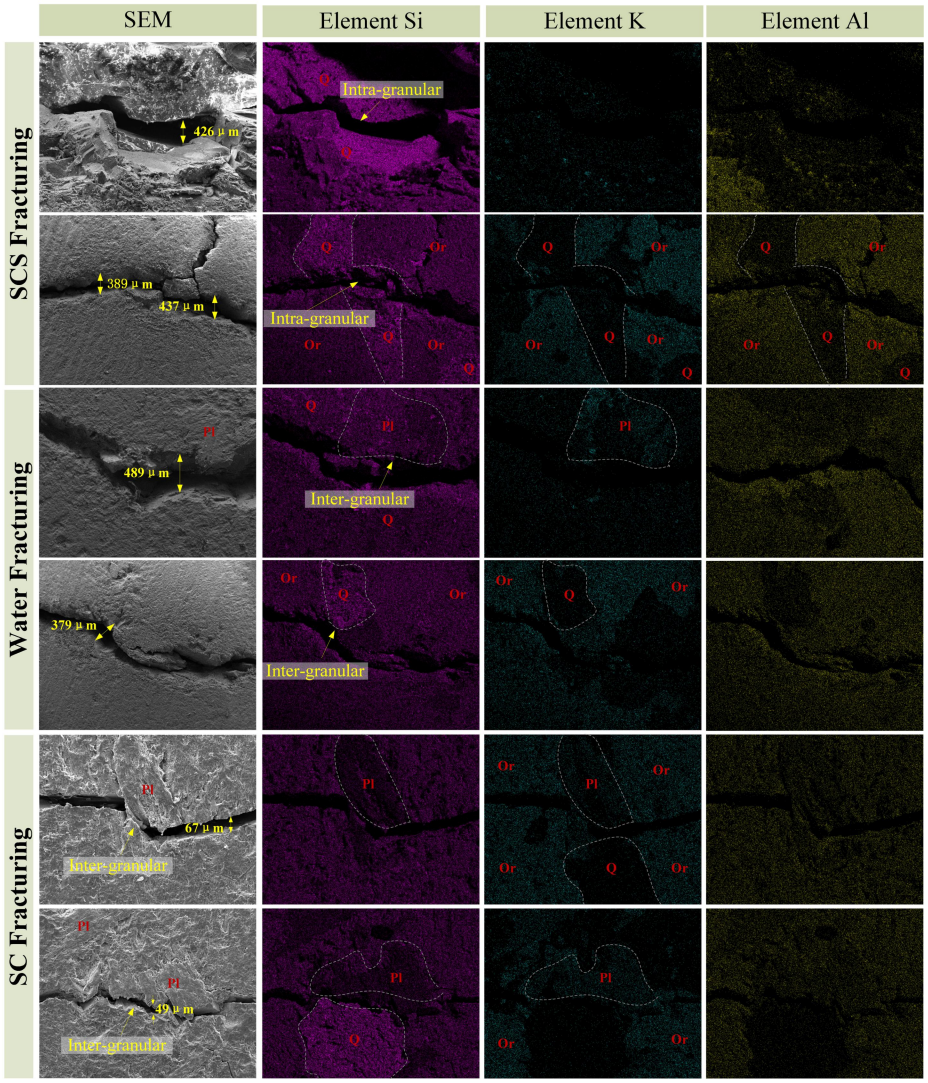

Fig. 10 SEM images of micro-failures of granites subjected to different fracturing methods. Q: quartz; Or: orthoclase; Pl: plagioclase. Orthoclase and plagioclase are aluminosilicate mineral containing elements of Al, Si and K, among which K is the main feature element in EDS. Compared to orthoclase, plagioclase has a striped structure. Quartz has higher abundance in Si elements in the EDS images.

3.4 Fracture morphology characterization

Fracture conductivity is a measure of the property of a fracture to convey the produced fluids of the well, and is measured in terms of permeability and average fracture width. High-conductivity fracture is desirable for EGS, which allows greater flow fluxes and achieves better heat extraction performances. Herein, reinjection tests of water were performed on the fractured granite without confining stress, to calculate and compare the conductivity of the fracture networks after different fracturing. The equation for the fracture conductivity C_f in the reinjection tests is given by the literature [36]:

$$C_f = \frac{25 q_w \mu \ln\left(\frac{r_e}{r_w}\right)}{3\pi \Delta P_{wf}}$$

where q_w is the injection rate, ml/min; μ is the viscosity of reinjection fluid, which is water in our work, mPa·s; r_e represents the effective radius, which is the half side-length of the samples in this work, mm; r_w is the wellbore radius, mm; ΔP_{wf} is the pressure difference between the wellbore and fracture, Mpa.

The calculation results of fracture conductivity for granites subjected to different fracturing are illustrated in Fig. 11. As compared to room-temperature granites (25 ℃), the high-temperature granite has higher fracture conductivity for a given fracturing method. Although the SC fracturing can create more tortuous fractures, the fractures induced by the quasi-static loading mode of CO2 are relatively narrow and thereby have relatively lower conductivity. At the rock temperature of 25℃ and 100℃, the conductivity of SC

fracturing is even lower than that of water fracturing. In contrast, in the SCS fracturing, a short dynamic impact pressure is applied to the granite. As a typical brittle material, rock is more prone to collapse under dynamic loading, thus SCS fracturing could generate a large-scale stimulation area with greater fracture width and higher fracture conductivity. The fracture conductivity of SCS fracturing is 3.4~7.0 times and 4.5~21.2 times higher than that of water fracturing and SC fracturing, respectively.

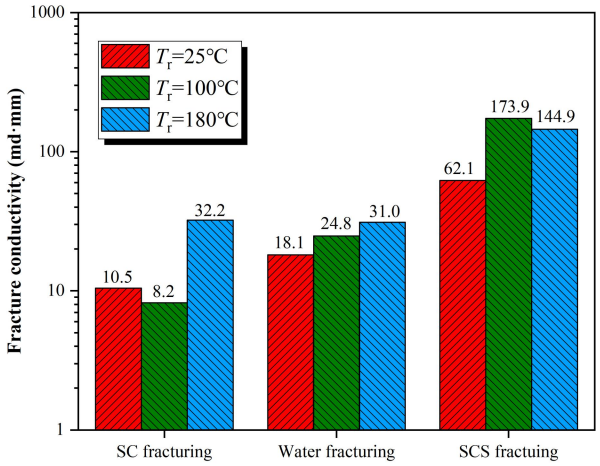

Fig. 11 Conductivity of fracture network in granites treated by different fracturing methods.

3.5 *Fracture morphology characterization*

In-situ stress is one of the important parameters affecting fracture morphology and complexity. The fracture propagation of traditional fracturing methods is usually significantly controlled by in-situ stress, so the fracture morphology and propagation direction are relatively simple, which characterized by single two-wing fracture. Regarding to SCS fracturing, in-situ stress plays a relatively weak role in controlling fracture propagation, unless the coefficient of horizontal stress difference is extremely high like SCS 4-1 shown in Fig. 12. Under low or moderate horizontal stress difference coefficients, such as SCS 3-3 and SCS 4-2 in Fig. 12, fracture propagation is random in direction, forming complex fractures with multiple branches. Taking the well-known FORGE site HDR geothermal reservoir as an example, the in-situ stress magnitudes in the field is σ_h=13.1~14.2 kPa/m and σ_H=13.1~14.2 kPa/m, with the coefficient of horizontal stress difference ranging in 0.08~0.41 [37], which falls in the low to moderate level. Hence, it is possible to create complex fractures with multiple branches and high conductivity in the dry hot rock reservoir by SCS fracturing.

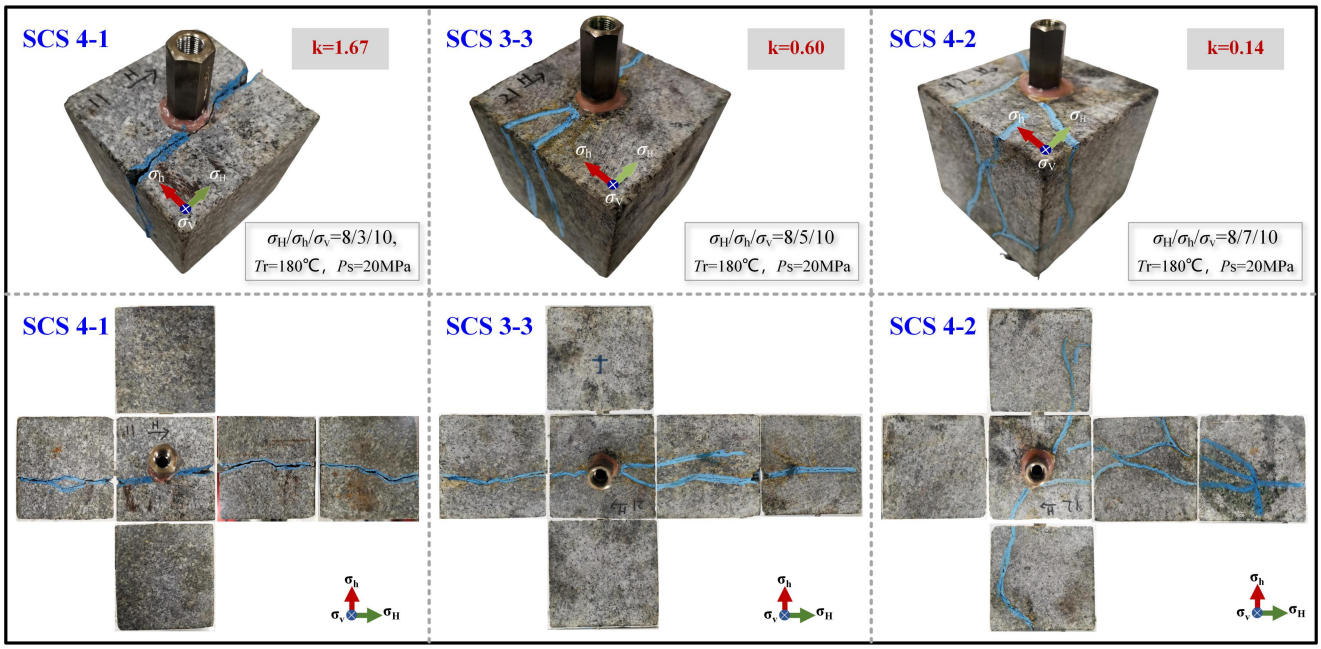

Fig. 12 Fracture patterns of granites subjected to SC-CO_2 shock fracturing under different tri-axial stress conditions.

In addition to the in-situ stress, shock pressure is also an important factor that determines the complexity of fracture morphology. The control degree of in-situ stress on the fracture patterns is closely related to the amplitude of the shock pressure in SCS fracturing. Fig. 13 shows the fracture propagation patterns of granites subjected to different shock pressures under the same stress conditions. Under the conditions of low shock pressure (14 and 16Mpa) like SCS 1-1 and 1-2, SCS fracturing created a single two-wing fracture along the

direction of maximum principal stress, in which cases the fracture propagation is dominated by the in-situ stress. However, as the shock pressure increases, the control of in-situ stress on fracture patterns becomes less dominant, and the number of branches and complexity of fractures improves significantly. Multiple fracture branches randomly intersected with the main fractures are generated at the shock pressure >18Mpa, as shown in SCS 1-3~1-5 in Fig. 13, due to the stronger dynamic impact loading effect. These branch fractures can greatly expand the stimulation area and improve the permeability of HDR reservoir. Thus, increasing shock pressure is beneficial to enhance the fracturing performance of SCS, and promote the fracture to get rid of the control of in-situ stress, forming a complex fracture network with multiple branches.

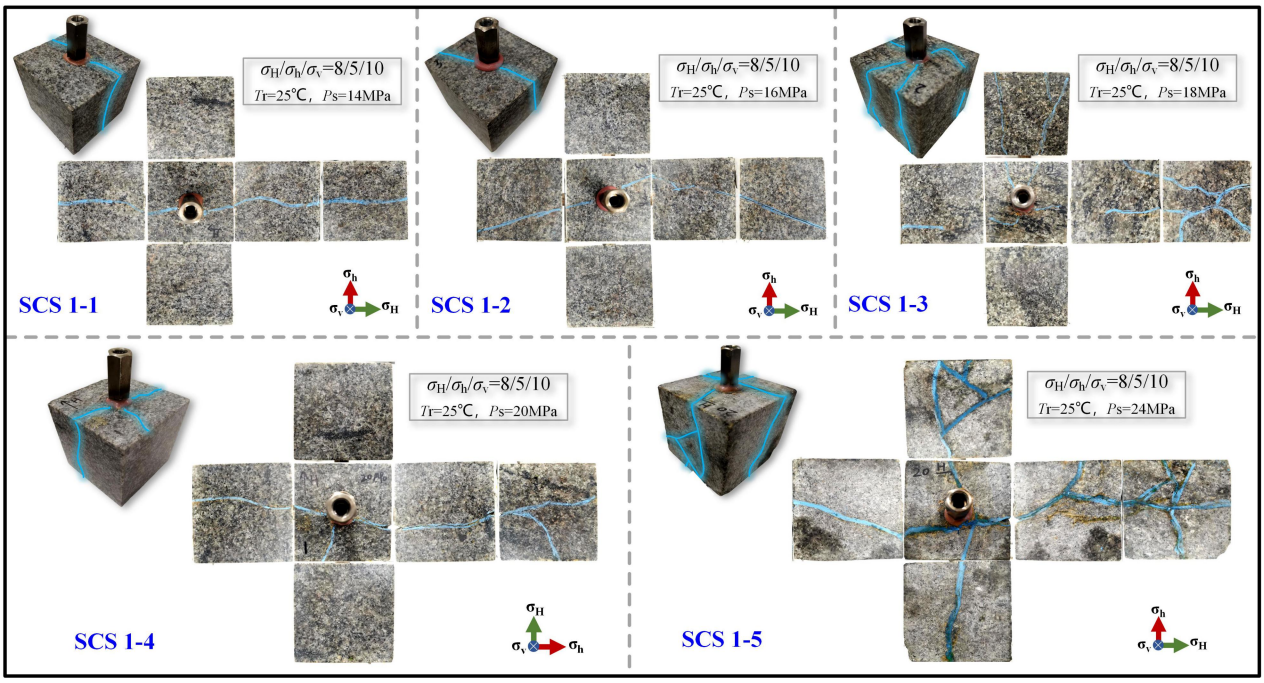

Fig. 13 Fracture patterns of granites subjected to SC-CO_2 shock fracturing under different shock pressures.

4. DISCUSSIONS

Granite, as a typical brittle material, has lower resistance to the dynamic impact loading. The basic idea of SCS fracturing is to create complex multi-branch fracture network and enhance the permeability of reservoir by inducing transient high-pressure impact waves, which is similar to the blasting fracturing and liquid CO_2 phase-transition fracturing (also referred as high-energy gas explosion fracturing). However, as compared to these two fracturing methods, SCS fracturing has significant differences in blasting pressure amplitude, loading rate and working period, as shown in Fig. 14. Blasting fracturing and liquid CO_2 explosive fracturing may have higher blasting pressure and faster loading rate, but they are generally disposable with only one round impact wave, limiting the extending length of fractures. Besides, the blasting medium in the explosion tubes is sensitive to external conditions and could be easily activated under the high-temperature and high-pressure conditions, thereby poses challenges to the application in HDR geothermal. In contrast, the SCS fracturing is a safer and more effective stimulation methods which could implement multi-round impact and eliminate the pre-detonation risks of explosive medium at high-temperature and high-pressure conditions during delivering in the wellbore. The relatively lower blasting pressure of SCS fracturing allows for the cyclic loading of dynamic shock through a specially designed device. In SCS fracturing, CO_2 is continuously injected into the specially designed downhole energizing device by using the fracturing pipes, instead of pre-sealing medium in the blasting tubes and delivering into downhole like blasting fracturing and liquid CO_2 phase-transition fracturing. Once the accumulated pressure exceeds the threshold value (about 100Mpa), the drainage channels of the downhole devices are opened to release high-pressure shock waves instantly. After pressure release, the pressure relief valve is automatically reset by the mechanical structure in the device, to repeat the energy accumulation and release process, implementing cyclic

high-pressure dynamic shock loading. Unlike the single round shock, multiple cyclic shocks benefit to further improve the complexity and conductivity of fractures, activate nature fractures by inducing alternate in-situ stress, and extend the stimulation area and corresponding heat extraction volume in the HDR reservoir significantly.discussion.

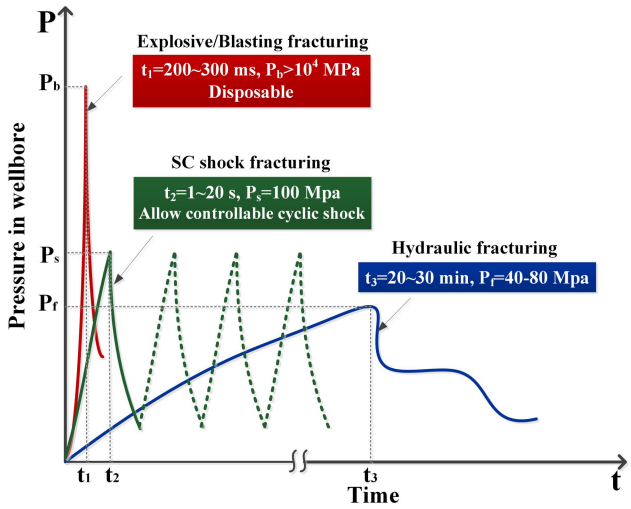

Fig. 14 Comparison in pressure evolution between different fracturing methods.

Although the shock pressure generated by SCS fracturing is not as high as that caused by blasting and phase transition fracturing, the energy generated by SCS fracturing is still quite considerable. According to the blasting theory, the blasting energy E and corresponding explosion equivalent W_{TNT} can be calculated as [38]:

$$E = \frac{PV}{k-1}\left[1-\left(\frac{0.1013}{P}\right)^{\frac{k-1}{k}}\right]\times 10^3$$

$$W_{TNT} = \frac{E}{Q_{TNT}}$$

where P is the shock pressure, MPa; V is the volume of blasting tube, m^3; k is the adiabatic coefficient, which is 1.295; Q_{TNT} is the explosion energy of 1kg trinitrotoluene (TNT), which is 4250 kJ/kg. Given the shock pressure of 100MPa, the energy released in single SCS fracturing is 311KJ, equivalent to 0.075kg of TNT explosive yield. After 20 cycles, 1.5kgTNT equivalent of energy can be released. With such high released energy, granite could be seriously cracked, generating complex multi-branch fractures in HDR reservoir.

Compared to hydraulic fracturing that characterized by quasi-static loading and typical two-wing straight fracture planes, SCS fracturing has the following advantages in the stimulation of HDR reservoirs: ① Instantaneous dynamic shock loading can crush the near-wellbore zone dramatically (zone A as shown in Fig. 15) to create a complex interconnected fracture network with high conductivity in a certain distance (a few meters to tens of meters as reported by Hu et al. [39]) around the wellbore. This zone significantly reduces the skin factor and corresponding flow resistance near the wellbore, enhancing the injection capacity and production rate of heat extraction fluid. High injection capacity of working medium is the key parameter to measuring the effectiveness of an EGS system. It is believed that EGS could be economically developed only when the injection capacity reaches 50L/s [16]. ② After forming zone A, subsequent injection of SC-CO_2 with cyclic shock further promotes the propagation of fractures and expands the stimulation areas, generating several extended main fractures with multiple secondary fractures (zone B in Fig. 15). These extended artificial fractures interconnect with natural fractures and joints in the geothermal reservoir, which improves the seepage and heat transfer spaces greatly. ③ Furthermore, continuous cyclic shock waves will cause disturbance of in-situ stress in the formation, change the stress state at natural fractures or joints, and activate them by inducing shear slip and self-prop between unconformable fracture surface [40, 41], and thereby further improve the permeability of the HDR formation. The success of the Soultz project in France has demonstrated that effective activation and utilization of natural fractures is critical for EGS stimulation in HDR geothermal [42]. Given all these, by forming a central crushing zone “A” characterized by a complex artificial fracture network and a fracture propagation zone “B” with multiple external extended artificial fractures interconnected by a large number of activated self-propped natural fractures and or joints, the SCS fracturing could address the fast thermal breakthrough issue induced by conventional hydraulic fracturing and prolong the heat recovery period greatly. Additionally, as a non-aqueous stimulation method, the SCS fracturing also offers advantages in environmental protection, carbon storage and utilization, achieving low-carbon solutions. Therefore, this technique may have a good application prospect for the stimulation of HDR geothermal in a more environmentally and more efficient way.

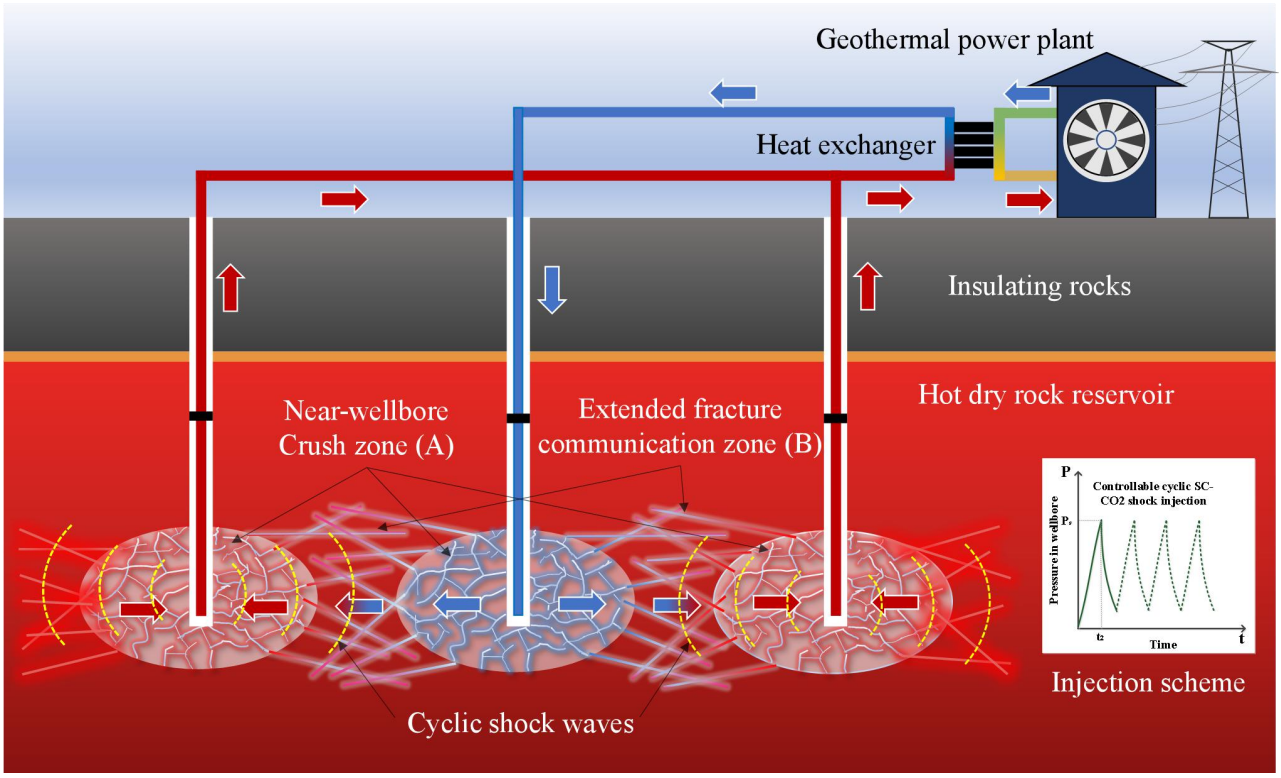

Fig. 15 Schematic of enhanced geothermal system created by SCS fracturing in HDR geothermal reservoir.

5. CONCLUSIONS

In this paper, controllable SC-CO_2 shock fracturing tests were performed on high-temperature granites in a lab-scale enhanced geothermal system. By comparing with conventional water fracturing and SC-CO_2 fracturing, the fracture initiation behavior and stimulation performance of SCS fracturing were determined quantitatively based on CT scanning and reinjection tests, with respect to fracture morphology and conductivity, and effects of critical parameters were investigated as well. Scanning electron microscope (SEM) was also used to determine the micro-failures characteristic of hot dry rock. Main conclusions are as follow:

1. In the SCS fracturing, the borehole pressure reaches to the peak rapidly in hundred milliseconds, which is significantly shorter than those of water fracturing and SC fracturing. There are multiple short pressure plateaus in the curves due to the pressure wave reflection and hedging in the borehole. The breakdown pressure is 24.2~57.5% lower than the shock pressure during SCS fracturing, and it decreases with increasing rock temperature. As compared to the granite at 25℃, the breakdown pressure of granite at 180℃ reduces by 50.3%, 14.2% and 44.3% for water fracturing, SC fracturing and SCS fracturing, respectively.

2. Two characteristic zones are created by SCS fracturing, i.e. near-wellbore crush zone and fracture radial extension zone. In the former zone, the granite is cracked remarkably, and multiple fractures crossed each other to form a fracture network, greatly reducing the skin coefficient near the wellbore, which contributes to a significant growth in EGS injection capacity and corresponding heat recovery. In the later zone, multiple outward-radiating fractures are created, which will be further extended by the subsequent continuous injection to connect the injection well and production wells. These randomly radiating extended fractures could communicate with more natural fractures and greatly enlarge the heat extraction spaces.

3. SCS fracturing could generate a large-scale stimulation area with larger seepage spaces and higher fracture conductivity. As compared to water fracturing and SC fracturing, the fracture conductivity of SCS fracturing is 3.4~7.0 times and 4.5~21.2 times higher, respectively. The fractal dimension of SCS fracture is 4.7% higher than that of water fracture, indicating that the fracture complexity is higher. SCS fracturing results in significantly larger heat extraction space. According to the CT scanning, the volume, area and width of fractures by SCS fracturing are 545.3%, 98.4% and 126.3% higher than those of water fracturing, respectively. Flatness of fracture by SCS fracturing is an

order of magnitude higher than that of water fracturing. Therefore, the fractures formed by SCS fracturing are more likely to self-support in the shear slip process, which improves the conductivity of the fractures and the heat recovery effect.

4. Rock temperature has a positive effect on the stimulation performance of SCS fracturing. As the rock temperature increases, both the tortuosity and conductivity of fractures improve dramatically. High-temperature granites are more likely to form complex fracture networks under the same shock pressure, with more interconnected branches and larger seepage spaces created, indicating that the SCS fracturing may have a better applicability in HDR reservoirs. The complex fracture network with high tortuosity and high conductivity in SCS fracturing benefits to extend the flow path of working medium, enhance the heat transfer performances, and prolong the serving life of EGS in the HDR geothermal reservoir.

5. In-situ stress is an important parameter affecting fracture morphology and complexity. The fracture propagation of conventional water fracturing is usually significantly controlled by in-situ stress, so the fracture morphology and propagation direction are relatively simple, which characterized by single two-wing fracture plane. Regarding to SCS fracturing, in-situ stress plays a relatively weak role in controlling fracture propagation. Under low or moderate horizontal stress difference coefficients (0.14~0.60), the propagation of fractures behaves more randomly in direction, contributing to forming complex fractures with multiple branches, which is desirable for the stimulation of HDR geothermal.

6. The control degree of in-situ stress on the fracture patterns is closely related to the amplitude of shock pressure in SCS fracturing. Under the conditions of low shock pressure, the fracture propagation is dominated by the in-situ stress, in which cases SCS fracturing created a typical two-wing fracture along the direction of maximum principal stress. However, as the shock pressure increases, the control of in-situ stress on fracture patterns becomes less dominant, and the number of branches and complexity of fractures improves significantly. Multiple fracture branches randomly intersected with the main fractures are generated at the shock pressure >18Mpa due to the stronger dynamic impact loading effect. Higher shock pressure is beneficial to enhance the stimulation performance of SCS fracturing, and promote the fracture to get rid of the control of in-situ stress in EGS.

ACKNOWLEDGEMENT

This work was supported by national Natural Science Foundation of China (No. 52204019, No.52192624), Science Foundation of China University of Petroleum, Beijing (No. 2462022QZDX005).

DECLARATION OF INTEREST STATEMENT

The authors declare that they have no known competing financial interests or personal relationships that could have appeared to influence the work reported in this paper. All authors read and approved the final manuscript.

REFERENCE

[1] Tester J, Anderson B, Batchelor A, et al. The future of geothermal energy[J]. Massachusetts Institute of Technology. 2006.

[2] Rybach L. Status and prospects of geothermal energy[C]. Proceedings world geothermal congress, 2010:1-5.

[3] Breede K, Dzebisashvili K, Liu X, Falcone G (2013) A systematic review of enhanced (or engineered) geothermal systems: past, present and future. Geotherm Energy 1:4

[4] Huenges E. Enhanced geothermal systems: Review and status of research and development[J]. Geothermal power generation, 2016, 743-61.

[5] Lu S M. A global review of enhanced geothermal system (EGS)[J]. Renewable and Sustainable Energy Reviews, 2018, 81: 2902-2921.

[6] Olasolo P, Juárez M, Morales M, et al. Enhanced geothermal systems(EGS): A review[J]. Renewable and Sustainable Energy Reviews, 2016, 56:133-44.

[7] POLLACK A, HORNE RN, MUKERJI T. What Are the Challenges in Developing Enhanced Geothermal Systems (EGS)? Observations from 64 EGS Sites[J]. 2020.

[8] Zhou Z, Jin Y, Zeng Y, et al. Investigation on fracture creation in hot dry rock geothermal formations of China during hydraulic fracturing[J]. Renewable Energy, 2020, 153: 301-313.

[9] Wu Y, Li P. The potential of coupled carbon storage and geothermal extraction in a CO2-enhanced geothermal system: a review[J]. Geothermal Energy, 2020, 8(1): 1-28.

[10] Zhang Z, Mao J, Yang X, et al. Advances in waterless fracturing technologies for unconventional reservoirs[J]. Energy Sources, Part A: Recovery, Utilization, and Environmental Effects, 2019, 41(2): 237-251.

[11] Feng C, Wang H, Jing Z. Investigation of heat extraction with flowing CO2 from hot dry rock by

numerical study[J]. Renewable Energy, 2021, 169: 242-253.
[12] Zhang W, Wang C, Guo T, et al. Study on the cracking mechanism of hydraulic and supercritical CO2 fracturing in hot dry rock under thermal stress[J]. Energy, 2021, 221: 119886.
[13] Shi Y, Song X, Shen Z, et al. Numerical investigation on heat extraction performance of a CO2 enhanced geothermal system with multilateral wells[J]. Energy, 2018, 163: 38-51.
[14] Yin T, Ma J, Wu Y, et al. Effect of high temperature on the brittleness index of granite: an experimental investigation[J]. Bulletin of Engineering Geology and the Environment, 2022, 81(11): 476.
[15] Van Everdingen A F. The skin effect and its influence on the productive capacity of a well[J]. Journal of petroleum technology, 1953, 5(06): 171-176.
[16] Dickson M H, Fanelli M. Geothermal energy: utilization and technology[M]. Routledge, 2013.
[17] Haizhu W, Gensheng L I, Yong Z, et al. Research status and prospects of supercritical CO2 fracturing technology[J]. Acta Petrolei Sinica, 2020, 41(1): 116.
[18] Middleton R S, Carey J W, Currier R P, et al. Shale gas and non-aqueous fracturing fluids: Opportunities and challenges for supercritical CO2[J]. Applied Energy, 2015, 147: 500-509.
[19] Zhang Y, Deng J, Ke B, et al. Experimental study on explosion pressure and rock breaking characteristics under liquid carbon dioxide blasting[J]. Advances in Civil Engineering, 2018, 2018.
[20] Cong R, Yang R, Wang H, et al. Supercritical CO2 Shock Fracturing on Coal: Experimental Investigation on Fracture Morphology and Pressure Characteristics[C]//56th US Rock Mechanics/Geomechanics Symposium. OnePetro, 2022.
[21] Shang Z, Wang H, Li B, et al. Experimental investigation of BLEVE in liquid CO2 phase-transition blasting for enhanced coalbed methane recovery[J]. Fuel, 2021, 292: 120283.
[22] Hu G, He W, Sun M. Enhancing coal seam gas using liquid CO2 phase-transition blasting with cross-measure borehole[J]. Journal of Natural Gas Science and Engineering, 2018, 60: 164-173.
[23] Ke B, Zhou K, Xu C, et al. Thermodynamic properties and explosion energy analysis of carbon dioxide blasting systems[J]. Mining Technology, 2019, 128(1): 39-50.
[24] Cui X, Ke B, Yu S, et al. Energy characteristics of seismic waves on Cardox blasting tube[J]. Geofluids, 2021, 2021: 1-13.
[25] Chen Y, Zhang H, Zhu Z, et al. A new shock-wave test apparatus for liquid CO2 blasting and measurement analysis[J]. Measurement and Control, 2019, 52(5-6): 399-408.
[26] Shang Z, Wang H, Li B, et al. Fracture processes in coal measures strata under liquid CO2 phase transition blasting[J]. Engineering Fracture Mechanics, 2021, 254: 107902.
[27] Wang B, Li H, Xing H, et al. Modelling of gas-driven fracturing and fragmentation in liquid CO2 blasting using finite-discrete element method[J]. Engineering Analysis with Boundary Elements, 2022, 144: 409-421.
[28] Zhu X, Jia J, Cai Z. Classification Method and Application of Rock Fracture Ability by Supercritical CO2 Blasting[J]. Shock and Vibration, 2022, 2022: 1-11.
[29] Shang Z, Wang H, Li B, et al. The effect of leakage characteristics of liquid CO2 phase transition on fracturing coal seam: applications for enhancing coalbed methane recovery[J]. Fuel, 2022, 308: 122044.
[30] Wang H, Cheng Z, Zou Q, et al. Elimination of coal and gas outburst risk of an outburst-prone coal seam using controllable liquid CO2 phase transition fracturing[J]. Fuel, 2021, 284: 119091.
[31] Gao X, Li T, Meng N, et al. Supercritical flow and heat transfer of SCO2 in geothermal reservoir under non-Darcy's law combined with power generation from hot dry rock[J]. Renewable Energy, 2023.
[32] Mahmoodpour S, Singh M, Bär K, et al. Thermo-hydro-mechanical modeling of an enhanced geothermal system in a fractured reservoir using carbon dioxide as heat transmission fluid-A sensitivity investigation[J]. Energy, 2022, 254: 124266.
[33] Pruess K. Enhanced geothermal systems (EGS) using CO2 as working fluid—A novel approach for generating renewable energy with simultaneous sequestration of carbon[J]. Geothermics, 2006, 35(4): 351-367.
[34] Zhang W, Wang C, Guo T, et al. Study on the cracking mechanism of hydraulic and supercritical CO2 fracturing in hot dry rock under thermal stress[J]. Energy, 2021, 221: 119886.
[35] Luo F, Xu R N, Jiang P X. Numerical investigation of fluid flow and heat transfer in a doublet enhanced geothermal system with CO2 as the working fluid (CO2–EGS)[J]. Energy, 2014, 64: 307-322.
[36] Yang R, Hong C, Liu W, et al. Non-contaminating cryogenic fluid access to high-temperature resources: Liquid nitrogen fracturing in a lab-scale Enhanced Geothermal System[J]. Renewable Energy, 2021, 165: 125-138.

[37] EGI, Frontier Observatory for Research in Geothermal Energy Milford Site, Utah - Phase 2B Final Topical Report, University of Utah, University of Utah, 2018.
[38] Karlos V, Solomos G. Calculation of blast loads for application to structural components[J]. Luxembourg: Publications Office of the European Union, 2013: 5.
[39] Hu X, Zhang R, Zhang B, et al. A Study on the Factors Influencing Coal Fracturing Range Caused by Liquid Carbon Dioxide Phase Transition[J]. Geofluids, 2022, 2022.
[40] Ma W, Wang Y, Wu X, et al. Hot dry rock (HDR) hydraulic fracturing propagation and impact factors assessment via sensitivity indicator[J]. Renewable Energy, 2020, 146: 2716-2723.
[41] Dehghan AN, Goshtasbi K, Ahangari K, et al. The effect of natural fracture dip and strike on hydraulic fracture propagation[J]. International Journal of Rock Mechanics and Mining Sciences, 2015, 100(75):210-5.
[42] Genter A, Evans K, Cuenot N, et al. Contribution of the exploration of deep crystalline fractured reservoir of Soultz to the knowledge of enhanced geothermal systems (EGS) [J]. Comptes Rendus Geoscience, 2010, 342(7-8):502-16.